Size-dependent second-harmonic generation from gold nanoparticles

Antonio Capretti,[1,2,*] Emanuele F. Pecora,[2,†] Carlo Forestiere,[1,2] Luca Dal Negro,[2,‡] and Giovanni Miano[1,§]

[1]*Department of Electrical Engineering and Information Technology, Università degli Studi di Napoli Federico II, Via Claudio 21, 80125 Napoli, Italy*

[2]*Department of Electrical and Computer Engineering & Photonics Center, Boston University, 8 Saint Mary's Street Boston, Massachusetts 02215, United States*

(Received 14 July 2013; revised manuscript received 7 November 2013; published 11 March 2014)

We experimentally and theoretically investigated the second-harmonic (SH) radiation from spherical gold nanoparticles as function of the particle radius in the range from 40 to 100 nm. By fitting the measured SH intensity to an analytical model, we demonstrated size-dependent second-order susceptibility tensor components, which significantly increase by reducing the size of the particles. Finally, we found new SH polarization diagrams for large particle radii arising from the interference among the different multipolar terms.

DOI: 10.1103/PhysRevB.89.125414 PACS number(s): 78.67.Bf, 42.25.Hz, 42.65.Ky, 73.20.Mf

Nonlinear optical phenomena have been extensively investigated in last decades. Fundamental light-matter interactions can be unveiled, and novel on-chip optical functionalities enabled. Efficient high-order harmonic generation, frequency mixing, wavelength converters, optical switches, and modulators can be engineered for innovative applications [1,2]. Noble metals such as Au, Ag, and Al may exhibit strong nonlinear response at optical frequencies. In fact, intense electric fields are generated at metal surfaces because of plasmonic oscillations, which enhance the nonlinear response [3–7].

Second harmonic (SH) generation is a frequency doubling process in which two photons (generally in the near-IR) interact in a nonlinear material and one photon (in the visible) is generated [1]. SH generation from nanostructured metals has received wide interest in the last few years. The dependence of the SH radiation on the polarization of the pump beam and the particle shape has been addressed for metallic colloids as well as for planar arrays of nanoparticles on a substrate [8–21].

Both the bulk and the surface of the metal contribute to the SH generation from noble metals nanoparticles. In particular, the bulk contribution has a nonlocal origin because of the material centrosymmetry, whereas the surface contribution is of local type [22–26]. In the Rayleigh limit ($R \ll \lambda/2\pi$) the SH radiation generated from the nanoparticle is dominated by both dipolar and quadrupolar components. Both the nonlocal-bulk and the local-surface SH sources contribute to the induced SH electric dipole moment, while only the local surface sources contribute to the induced SH electric quadrupole moment [10,27]. As the nanoparticle radius increases, a SH octupole component arises. Evidence of interference effects between the SH dipolar and octupolar sources have been reported for nanoparticles of fixed size [13,14]. Recently, using the nonlinear Mie theory we have theoretically predicted that SH dipole-octupole interference would provide a wide variety of patterns in the p component [28].

The SH signal dependence on the particle size has been investigated in the past years for polymer colloids with radii in the 100 nm to 1.5 μm range [29,30]. In Ref. [10], the SH response has been investigated for gold nanoparticles with radii in the 5 to 75 nm range. The hyperpolarizability tensor is commonly used to characterize the SH radiation from nanoparticles in the small-particle limit. However, if retardation effects become important, a description based on the second-order susceptibility tensor is necessary [27,28]. An alternative approach makes use of an effective susceptibility to describe nonlinear scattering of arbitrary order [31]. Recently, the important components of the susceptibility tensor have been experimentally evaluated for gold spherical nanoparticles of radius $R = 75$ nm [14]. However, the role played by the nanoparticle size on the SH generation process, as well as the experimental determination of the second-order susceptibility tensor are still open issues.

In this paper, we investigate the SH generation from gold colloids as the nanoparticle radius varies in the range from 40 up to 100 nm. We quantify the second-order surface susceptibility components $\chi^{\text{equ}}_{\perp\perp\perp}$, $\chi^{\text{equ}}_{\perp\parallel\parallel}$, and $\chi_{\parallel\perp\parallel}$ by comparing the measured SH radiation patterns with rigorous predictions from the nonlinear Mie theory [28]. This study demonstrates that the second-order susceptibility tensor components of gold nanoparticles is significantly increased by reducing their size.

We have measured the SH radiation generated from a set of commercial (BBI Solutions) monodispersed gold colloids in pure water (with residual chemical concentration of 0.01%). The nanoparticle shape is spherical with radii 40, 50, 75, and 100 nm, and with a size variation less than 8%. The experimental setup is sketched in Fig. 1(a). Gold colloids are excited by a pulsed Ti:Sapphire laser (MaiTai HP Spectra Physics, 150 fs pulse width, 12 nJ pulse energy, 82 MHz repetition rate) operated at $\lambda = 800$ nm and $\lambda = 840$ nm, and propagating along the z axis. Gold colloids in the investigated size range show plasmon resonance peaks in the 500 to 650 nm wavelength range, where neither the pump laser nor the second-harmonic wavelengths are located. The laser output is linearly polarized and we rotate the polarization in the xOy plane, using a half-wave liquid crystal variable retarder (Thorlabs LCC1111-B); α is the angle formed by the direction of the electric field with the x axis [Fig. 1(b)]. The beam is focused onto the colloidal solution through a

*Present address: CNR-SPIN, Complesso MonteSantangelo Via Cinthia, 80126 Napoli, Italy.

†Present address: Department of Materials Science and Engineering, Stanford University, Stanford California 94305, USA.

‡dalnegro@bu.edu

§miano@unina.it

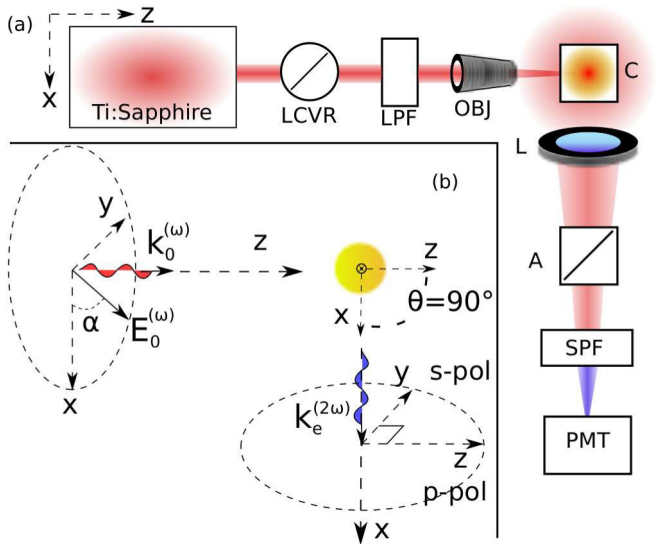

FIG. 1. (Color online) (a) Experimental setup: Ti:sapphire ultrafast laser, liquid crystal variable retarder (LCVR), low-pass filter (LPF), objective (OBJ), gold colloids (C), lens (L), analyzer (A), short-pass filter (SPF), detector (PMT). (b) Excitation-collection configuration: the pump beam $\boldsymbol{k}_0^{(\omega)}$ propagates along the z axis and is linearly polarized in the xOy plane (α is the angle between the x-axis and the electric field $\boldsymbol{E}_0^{(\omega)}$). The signal is collected along the x axis and its p and s components, with respect to the scattering plane xOz, are analyzed.

20× microscope objective. We measure the intensity of the SH radiation generated by the nanoparticles along the x axis, i.e., the excitation and the collection directions form an angle $\theta = 90^\circ$. The signal output is collected by a 30 mm lens and coupled into an $f/4$ monochromator (Cornerstone 260). The pump light was rejected by a 650 nm short-pass filter placed in front of the monochromator slits, along with a polarization analyzer. The SH spectra have been detected with a lock-in amplifier (Oriel Merlin) coupled to a low-light photomultiplier tube (PMT, Oriel Instrumentation 77348). Absolute values of the SH power have been measured using the procedure already discussed elsewhere [32,33].

This excitation-collection configuration has the remarkable property that it allows for the separation of the radiation generated from different multipoles of the SH source. In particular, the collected SH radiation is analyzed in its p and s components with respect to the xOz scattering plane; namely, the intensity of the SH electric field components along the z and the y axis, as shown in Fig. 1(b). The odd-order multipoles only contribute to the p component (along the z axis) of the SH signal, whereas the even-order multipoles only contribute to the s component (along the y axis) [28].

The sources of SH radiation in centrosymmetric nanoparticles can be represented by a nonlinear polarization induced by the electromagnetic field $\boldsymbol{E}^{(\omega)}$ at the fundamental frequency ω [27,28]. This nonlinear polarization is composed by a local contribution $\mathbf{P}_s^{(2\omega)}$ on the particle surface Σ [22]:

$$\mathbf{P}_s^{(2\omega)} = \varepsilon_0 \overleftrightarrow{\chi}_s^{(2)} : \mathbf{E}^{(\omega)}\mathbf{E}^{(\omega)}, \tag{1}$$

where $\boldsymbol{E}^{(\omega)}$ is the electric field at the fundamental frequency at the inner face of Σ, and a nonlocal contribution $\mathbf{P}_b^{(2\omega)}$ in the particle bulk [23]:

$$\mathbf{P}_b^{(2\omega)} = \varepsilon_0 \overleftrightarrow{\chi}_b^{(2)} : \mathbf{E}^{(\omega)} \nabla \mathbf{E}^{(\omega)}, \tag{2}$$

where $\overleftrightarrow{\chi}_s^{(2)}$ and $\overleftrightarrow{\chi}_b^{(2)}$ are the corresponding surface and bulk second-order susceptibility tensors, respectively, and ε_0 is the vacuum permittivity. Since the nanoparticle surface possesses isotropic symmetry with a mirror plane perpendicular to it, the second-order surface susceptibility $\vec{\chi}_s^{(2\omega)}$ has only three nonvanishing and independent components, $\chi_{\perp\perp\perp}$, $\chi_{\perp\parallel\parallel}$, and $\chi_{\parallel\perp\parallel} = \chi_{\parallel\parallel\perp}$, where $\perp$ and $\parallel$ refer to the orthogonal and tangential components to the particle surface [22]. Therefore Eq. (1) reduces to

$$\begin{aligned}\mathbf{P}_s^{(2\omega)} = \varepsilon_0 [&\chi_{\perp\perp\perp} \hat{\mathbf{n}}\hat{\mathbf{n}}\hat{\mathbf{n}} + \chi_{\perp\parallel\parallel}(\hat{\mathbf{n}}\hat{\mathbf{t}}_1\hat{\mathbf{t}}_1 + \hat{\mathbf{n}}\hat{\mathbf{t}}_2\hat{\mathbf{t}}_2) \\ &+ \chi_{\parallel\perp\parallel}(\hat{\mathbf{t}}_1\hat{\mathbf{n}}\hat{\mathbf{t}}_1 + \hat{\mathbf{t}}_2\hat{\mathbf{n}}\hat{\mathbf{t}}_2)] : \mathbf{E}^{(\omega)}\mathbf{E}^{(\omega)},\end{aligned} \tag{3}$$

where $\hat{\mathbf{n}}$ is the normal to the particle surface pointing outward and $\hat{\mathbf{t}}_1$, $\hat{\mathbf{t}}_2$ are two orthonormal vectors defining the plane tangent to the particle surface, such that $(\hat{\mathbf{n}},\hat{\mathbf{t}}_1,\hat{\mathbf{t}}_2)$ is a counterclockwise triad. Moreover, since noble metals are isotropic homogeneous media, the second-order bulk susceptibility $\vec{\chi}_b^{(2)}$ can be written as [22,27]

$$\mathbf{P}_b^{(2\omega)} = \varepsilon_0 \gamma \nabla(\mathbf{E}^{(\omega)} \cdot \mathbf{E}^{(\omega)}) + \varepsilon_0\, \delta'(\mathbf{E}^{(\omega)} \cdot \nabla)\mathbf{E}^{(\omega)}, \tag{4}$$

where γ and δ' are material parameters [22]. The second contribution in Eq. (4) has been neglected in Ref. [14], and it has been experimentally demonstrated to be smaller than the other contributions in Ref. [34] for a gold film. This contribution is ineffectual in the experimental configuration of our experiment, as demonstrated in the Supplemental Material [35]. It is also well known that the contribution of the term γ to the SH radiation at the external of the particle may be described through the equivalent surface sources $[\gamma\varepsilon_0/\varepsilon_i(2\omega)] \cdot [\hat{\boldsymbol{n}}\hat{\boldsymbol{n}}\hat{\boldsymbol{n}} + \hat{\boldsymbol{n}}(\hat{\boldsymbol{t}}_1\hat{\boldsymbol{t}}_1 + \hat{\boldsymbol{t}}_2\hat{\boldsymbol{t}}_2)]$ [22,28]. Consequently, we consider a sphere with only surface SH sources described through the equivalent second-order surface susceptibility components [28,34]:

$$\chi_{\perp\perp\perp}^{\text{equ}} = \chi_{\perp\perp\perp} + \gamma\varepsilon_0/\varepsilon_i(2\omega)\,, \tag{5}$$

$$\chi_{\perp\parallel\parallel}^{\text{equ}} = \chi_{\perp\parallel\parallel} + \gamma\varepsilon_0/\varepsilon_i(2\omega)\,, \tag{6}$$

$$\chi_{\parallel\perp\parallel} = \chi_{\parallel\parallel\perp}\,. \tag{7}$$

We estimate the equivalent second-order surface susceptibility components $\chi_{\perp\perp\perp}^{\text{equ}}$, $\chi_{\perp\parallel\parallel}^{\text{equ}}$, and $\chi_{\parallel\perp\parallel}$ by measuring the SH intensity scattered by the gold colloids. In particular, we minimize the root-mean-square deviation (RMSD) between the experimental and analytical distribution of the SH radiated power per unit solid angle $dP_{\hat{\varepsilon}^*}^{(2\omega)}(\hat{\mathbf{x}})/d\Omega$ at the collection direction [see Fig. 1(b)], as the α angle varies from 0° to 360°. The analytical expression of $dP_{\hat{\varepsilon}^*}^{(2\omega)}(\hat{\mathbf{x}})/d\Omega$ is obtained by solving the second-harmonic Mie scattering problem for the equivalent sphere. The theory of nonlinear Mie scattering has been developed in the last decade (see for instance Refs. [36–39] and references therein). Here we follow the formulation of Ref. [28], in which we consider all the local-surface and nonlocal-bulk SH sources relevant to metal nanoparticles. The SH electromagnetic field is expanded in terms of spherical vector

wave functions (SVWFs) $\{\mathbf{M}_{mn}^{(J)}(kr,\theta,\phi),\mathbf{N}_{mn}^{(J)}(kr,\theta,\phi)\}$, where (r,θ,ϕ) are spherical coordinates having origin at the sphere center and k is the wave number. The SH power per unit solid angle radiated along the x axis and collected through an analyzer with polarization state $\hat{\boldsymbol{\varepsilon}}^* = \hat{\boldsymbol{z}}$ (SH p component) and $\hat{\boldsymbol{\varepsilon}}^* = \hat{\boldsymbol{y}}$ (SH s component) is

$$\frac{dP_{\hat{\varepsilon}^*}^{(2\omega)}(\hat{\mathbf{x}})}{d\Omega} = \lim_{r\to\infty}\frac{\left|rE_c^{(2\omega)}\right|^2}{2\zeta_e}\left|\hat{\boldsymbol{\varepsilon}}^*\cdot\sum_{n=1}^{N}\sum_{m=-n}^{n} b_{mn}^{(2\omega)}\mathbf{M}_{mn}^{(3)}\left(k_e^{(2\omega)}r,\,\theta=\frac{\pi}{2},\,\phi=\mathbf{0}\right)+a_{mn}^{(2\omega)}\mathbf{N}_{mn}^{(3)}\left(k_e^{(2\omega)}r,\,\theta=\frac{\pi}{2},\,\phi=\mathbf{0}\right)\right|^2,$$

where $k_e^{(2\omega)}$ and ζ_e are, respectively, the wave number and the impedance of the external medium, $E_c^{(2\omega)}$ is a characteristic electric field [28], and N is the maximum order of SVWF used. The SH scattering coefficients $a_{mn}^{(2\omega)}$ and $b_{mn}^{(2\omega)}$ depend on the fundamental field wavelength λ, the polarization angle α, and the second-order nonlinear susceptibility. In particular $a_{mn}^{(2\omega)}$ and $b_{mn}^{(2\omega)}$ are linear functions of $\chi_{\perp\perp\perp}^{\text{equ}}$, $\chi_{\perp\parallel\parallel}^{\text{equ}}$, and $\chi_{\parallel\perp\parallel}$ and their analytical expressions are given in terms of the Clebsch-Gordan coefficients [28,40]. Due to the spherical symmetry, the coefficients $b_{mn}^{(2\omega)}$ only depend on $\chi_{\parallel\perp\parallel}$. The identification of the equivalent second-order susceptibility components is performed by setting $N = 10$. For the investigated particle size and incident wavelength, the non-negligible SH multipoles are the dipole ($n = 1$) and octupole ($n = 3$) for the SH p component, and the quadrupole ($n = 2$) for the s component.

In the small-particle limit (i.e., $R \ll \lambda/2\pi$), the SH p component is governed by the SH dipole, resulting in an intensity independent of the pump-polarization angle α [27]. In Fig. 2 we show the pump-polarization dependence of the SH p component at the pump wavelengths $\lambda = 800$ nm (top panels) and $\lambda = 840$ nm (bottom panels) obtained from measurements (points) and nonlinear Mie theory (lines), as we move away from the Rayleigh limit. The resulting RMSD is less than 10%. In the polarization diagrams shown in Figs. 2(a), 2(b), 2(e), and 2(f) a small octupolar component arises, and the interference between the SH dipole and octupole components results in a ellipsoidal pattern with maximum intensity for $\alpha = 90°$, as already shown in Ref. [13]. By further increasing the nanoparticle radius we observe in Figs. 2(c), 2(d), 2(g), and 2(h) the appearance of two maxima at $\alpha = 0°$ and $\alpha = 90°$. This variety of patterns in the p component is related to the interference between the dipole and octupole terms, depending on the particle size, as predicted in Ref. [28]. On the other hand, the pump-polarization dependence of the SH s component (not shown) is only dominated by radiation generated by the quadrupole component of the SH source, and no interference appears.

Figure 3 shows the maximum power of the measured p and s components (detected at $\alpha = 90°$ and $\alpha = 0°$, respectively) as a function of the particle radius for two values of the pump wavelength. The measured power has been normalized to the particle concentration for each size of gold colloids. The relative intensities of the p and s components significantly vary with the particle radius. The intensity of the s component is greater than the intensity of the p component for radii larger than 50 nm. The intensity of the p component increases monotonically whereas that of the s component shows a maximum around 75 nm. The peak position of the s component is expected to shift to larger particle radii when the pump wavelength is increased from $\lambda = 800$ nm to $\lambda = 840$ nm, in agreement with the theoretical analysis presented in Ref. [28].

Figure 4 shows the estimated components of the equivalent second-order surface susceptibility tensor as a function of the particle size and for two pump wavelengths. A clear trend versus the particle size can be observed. In particular, the components $\chi_{\perp\perp\perp}^{\text{equ}}$ and $\chi_{\parallel\perp\parallel}$ acquire their maximum value at the smallest investigated particle size and show a monotonic decrease when reducing the particle size, for both the incident wavelengths. On the contrary, the component $\chi_{\perp\parallel\parallel}^{\text{equ}}$ does not show a monotonic trend with the particle size, and it displays a maximum at a particle size that depends on the incident

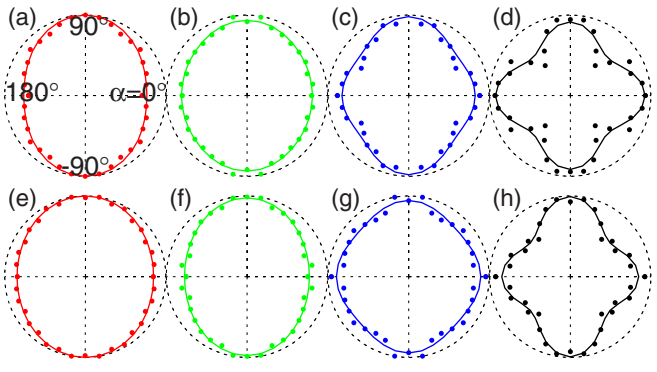

FIG. 2. (Color online) Intensity of the SH p component as function of the angle of polarization of the pump beam α, for (a), (e) $R = 40$ nm, (b), (f) $R = 50$ nm, (c), (g) $R = 75$ nm, and (d), (h) $R = 100$ nm. The pump wavelengths are (a)–(d) $\lambda = 800$ nm and (e)–(h) $\lambda = 840$ nm. Points are experimental data and lines are calculated values. Curves are not to scale.

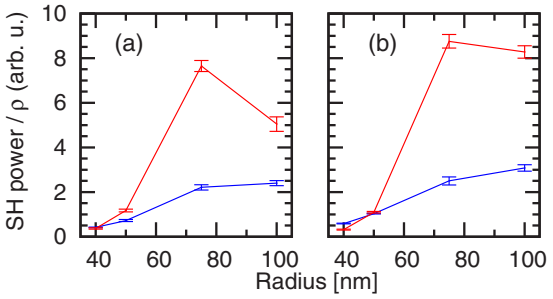

FIG. 3. (Color online) Maximum power of the measured p (blue) and s (red) components (detected at $\alpha = 90°$ and $\alpha = 0°$, respectively) as a function of the particle radius, at the pump wavelength (a) $\lambda = 800$ nm and (b) $\lambda = 840$ nm. The measured power has been normalized to the particle concentration ρ for each size of gold colloids.

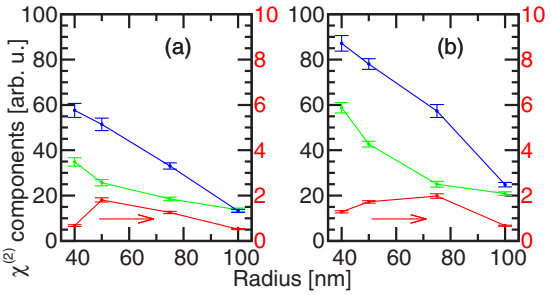

FIG. 4. (Color online) Components of the equivalent second-order surface susceptibility tensor as function of the nanoparticle size. Left-hand scale: $\chi^{equ}_{\perp\perp\perp}$ (blue) and $\chi_{\parallel\perp\parallel}$ (green); right-hand scale: $\chi^{equ}_{\perp\parallel\parallel}$ (red). The pump wavelengths are (a) $\lambda = 800$ nm and (b) $\lambda = 840$ nm.

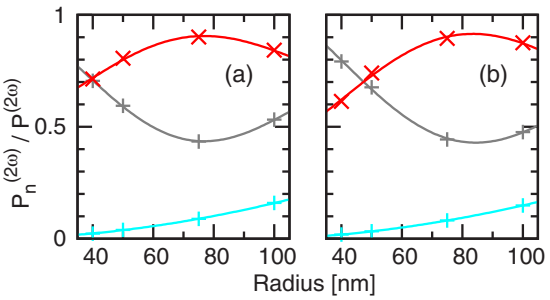

FIG. 5. (Color online) Contributions of the SH dipole (gray), quadrupole (red), and octupole (cyan) to the SH power as function of the gold nanoparticle size. The pump wavelengths are (a) $\lambda = 800$ nm and (b) $\lambda = 840$ nm. Continuous lines are a guide to the eye.

wavelength. However, its amplitude is up to two orders of magnitude smaller than the other two components. Since the SH sources $\chi^{equ}_{\perp\perp\perp}$ and $\chi^{equ}_{\perp\parallel\parallel}$ radiate in the same way [22], the contribution of the latter component to the SH radiation is negligible. In the framework of the hydrodynamic model for the SH generation from gold, $\chi_{\perp\parallel\parallel}$ is negligible and the γ bulk contribution is separable from the surface contributions $\chi_{\perp\parallel\parallel}$ and $\chi_{\perp\perp\perp}$ in Eqs. (5) and (6) [14,41].

The finite curvature of the particle surface, as well as the enhanced surface-to-volume ratio of smaller spheres, can explain the measured dependence of the second-order surface susceptibility tensor on the particle size. Moreover, the colloid solution can modify the properties of the gold surface [42–44].

Figure 5 shows the calculated multipolar contributions $P_n^{(2\omega)}/P^{(2\omega)}$ to the total SH power $P^{(2\omega)}$ radiated in all directions, for the orders $n = 1,2,3$. In the investigated size range, the SH contribution $P_1^{(2\omega)}/P^{(2\omega)}$ due to the SH dipole decreases as the particle size increases and shows a minimum at $R = 75$ nm. Analogously, the SH quadrupolar contribution $P_2^{(2\omega)}/P^{(2\omega)}$ increases with the particle size and displays a maximum at the same radius.

The SH octupolar term $P_3^{(2\omega)}/P^{(2\omega)}$, which is expected to be zero for $R \ll \lambda$, increases monotonically in the investigated size range. It is interesting to note that, although $P_3^{(2\omega)}/P^{(2\omega)}$ is always smaller than $P_1^{(2\omega)}/P^{(2\omega)}$ for the investigated nanoparticle radii, the interference between the two SH multipoles significantly modifies the pump-polarization dependence, as showed in Fig. 2. The deviation of the SH p component from a pure SH dipole has been experimentally investigated in the size range $R = 10$ to 50 nm by Bachelier *et al.* [13]. Here, we demonstrate that the SH octupole is not negligible with respect to the dipole for particle radii larger than $R = 75$ nm. The interference between the two multipoles gives rise to the distinctive interference patterns shown in Figs. 2(c), 2(d), 2(g), and 2(h).

In conclusion, we have experimentally and theoretically investigated the second-harmonic generation from gold nanospheres as a function of their radii. We demonstrated increased second-order susceptibility tensor components by reducing the size of the particles, along with the interference of different multipolar orders in the SH polarization diagrams.

Our findings unveil the importance of nonlinear surface contributions at the nanoscale and have a direct impact in the analysis and design of plasmon-enhanced nonlinear structures of interest to a number of engineering applications such as all-optical switchers, modulators and frequency converters.

This work was partly supported by the Italian Ministry of Education, University and Research through the project PON01_02782, by the AFOSR under Award FA9550-10-1-0019, by the NSF Career Award No. ECCS-0846651, and by the US Army Research Laboratory through the Collaborative Research Alliance (CRA) for MultiScale multidisciplinary Modeling of Electronic materials (MSME).

[1] Y. Shen, *The Principles of Nonlinear Optics* (Wiley-Interscience, Hoboken, NJ, 2003).
[2] R. Boyd, *Nonlinear Optics*, Nonlinear Optics Series (Elsevier Science, Oxford, UK, 2008).
[3] H. J. Simon, D. E. Mitchell, and J. G. Watson, Phys. Rev. Lett. **33**, 1531 (1974).
[4] C. K. Chen, A. R. B. de Castro, and Y. R. Shen, Phys. Rev. Lett. **46**, 145 (1981).
[5] J. C. Quail and H. J. Simon, Phys. Rev. B **31**, 4900 (1985).
[6] R. Murphy, M. Yeganeh, K. J. Song, and E. W. Plummer, Phys. Rev. Lett. **63**, 318 (1989).
[7] M. Kauranen and A. V. Zayats, Nat. Photon. **6**, 737 (2012).
[8] B. Lamprecht, A. Leitner, and F. Aussenegg, Appl. Phys. B **68**, 419 (1999).
[9] M. McMahon, D. Ferrara, C. Bowie, R. Lopez, and R. Haglund, Jr., Appl. Phys. B **87**, 259 (2007).
[10] I. Russier-Antoine, E. Benichou, G. Bachelier, C. Jonin, and P. F. Brevet, J. Phys. Chem. C **111**, 9044 (2007).
[11] Y. Zeng, W. Hoyer, J. Liu, S. W. Koch, and J. V. Moloney, Phys. Rev. B **79**, 235109 (2009).
[12] M. Scalora, M. A. Vincenti, D. de Ceglia, V. Roppo, M. Centini, N. Akozbek, and M. J. Bloemer, Phys. Rev. A **82**, 043828 (2010).

[13] J. Butet, G. Bachelier, I. Russier-Antoine, C. Jonin, E. Benichou, and P.-F. Brevet, Phys. Rev. Lett. **105**, 077401 (2010).
[14] G. Bachelier, J. Butet, I. Russier-Antoine, C. Jonin, E. Benichou, and P.-F. Brevet, Phys. Rev. B **82**, 235403 (2010).
[15] A. Benedetti, M. Centini, M. Bertolotti, and C. Sibilia, Opt. Express **19**, 26752 (2011).
[16] H. Aouani, M. Navarro-Cia, M. Rahmani, T. P. H. Sidiropoulos, M. Hong, R. F. Oulton, and S. A. Maier, Nano Lett. **12**, 4997 (2012).
[17] C. Ciraci, E. Poutrina, M. Scalora, and D. R. Smith, Phys. Rev. B **85**, 201403 (2012).
[18] A. Capretti, G. F. Walsh, S. Minissale, J. Trevino, C. Forestiere, G. Miano, and L. Dal Negro, Opt. Express **20**, 15797 (2012).
[19] S. G. Rodrigo, H. Harutyunyan, and L. Novotny, Phys. Rev. Lett. **110**, 177405 (2013).
[20] J. Butet, K. Thyagarajan, and O. J. F. Martin, Nano Lett. **13**, 1787 (2013).
[21] C. Forestiere, A. Capretti, and G. Miano, J. Opt. Soc. Am. B **30**, 2355 (2013).
[22] T. Heinz, in *Nonlinear Surface Electromagnetic Phenomena*, *Modern Problems in Condensed Matter Sciences*, edited by H. Ponath and G. Stegeman (North-Holland, Amsterdam, 1991), pp. 353–416.
[23] N. Bloembergen, R. K. Chang, S. S. Jha, and C. H. Lee, Phys. Rev. **174**, 813 (1968).
[24] G. Agarwal and S. Jha, Solid State Commun. **41**, 499 (1982).
[25] P. Guyot-Sionnest, W. Chen, and Y. R. Shen, Phys. Rev. B **33**, 8254 (1986).
[26] P. Guyot-Sionnest and Y. R. Shen, Phys. Rev. B **35**, 4420 (1987).
[27] J. I. Dadap, J. Shan, and T. F. Heinz, J. Opt. Soc. Am. B **21**, 1328 (2004).
[28] A. Capretti, C. Forestiere, L. Dal Negro, and G. Miano, Plasmonics **9**, 151 (2014).
[29] L. Schneider, H. Schmid, and W. Peukert, Appl. Phys. B **87**, 333 (2007).
[30] S.-H. Jen, G. Gonella, and H.-L. Dai, J. Phys. Chem. A **113**, 4758 (2009).
[31] S. Roke, M. Bonn, and A. V. Petukhov, Phys. Rev. B **70**, 115106 (2004).
[32] E. F. Pecora, A. Capretti, G. Miano, and L. Dal Negro, Appl. Phys. Lett. **102**, 141114 (2013).
[33] E. F. Pecora, G. F. Walsh, C. Forestiere, A. Handin, E. Russo-Averchi, A. Dalmau-Mallorqui, I. Canales-Mundet, A. Fontcuberta i Morral, and L. D. Negro, Nanoscale **5**, 10163 (2013).
[34] F. X. Wang, F. J. Rodriguez, W. M. Albers, R. Ahorinta, J. E. Sipe, and M. Kauranen, Phys. Rev. B **80**, 233402 (2009).
[35] See Supplemental Material at http://link.aps.org/supplemental/10.1103/PhysRevB.89.125414 for a discussion about the δ' bulk term.
[36] Y. Pavlyukh and W. Hübner, Phys. Rev. B **70**, 245434 (2004).
[37] A. G. F. de Beer and S. Roke, Phys. Rev. B **79**, 155420 (2009).
[38] G. Gonella and H.-L. Dai, Phys. Rev. B **84**, 121402 (2011).
[39] S. Wunderlich, B. Schürer, C. Sauerbeck, W. Peukert, and U. Peschel, Phys. Rev. B **84**, 235403 (2011).
[40] D. Varshalovich, A. Moskalev, and V. Khersonski, *Quantum Theory of Angular Momentum* (World Scientific, Singapore, New Jersey, Hong Kong, 1988).
[41] J. E. Sipe, V. C. Y. So, M. Fukui, and G. I. Stegeman, Phys. Rev. B **21**, 4389 (1980).
[42] B. Schürer, S. Wunderlich, C. Sauerbeck, U. Peschel, and W. Peukert, Phys. Rev. B **82**, 241404 (2010).
[43] S. Roke and G. Gonella, Annu. Rev. Phys. Chem. **63**, 353 (2012).
[44] N. Gomopoulos, C. Lütgebaucks, Q. Sun, C. Macias-Romero, and S. Roke, Opt. Express **21**, 815 (2013).